Dalton Transactions

PAPER

Check for updates

Influence of the even–odd effect on the crystal structure, band structure and optical properties of hybrid crystals of the [H₃N-(CH₂)ₙ-NH₃]PbX₄ (*n* = 4–8 and X = Cl, Br, and I) type†

Mikhail I. Balanov,[a] Alexei V. Emeline[b] and Dmitry S. Shtarev ⓘ *[c]

In the presented work, the structure dependence as well as luminescence features of a wide range of hybrid crystals based on lead halides and a homologous series of alkyl diamines from 1,4-diaminobutane to 1,8-diaminooctane are investigated. The structure of several previously undescribed hybrid crystals has been established. The even–odd effect of alkanes and its influence on the structure of such hybrid crystals have been demonstrated for the first time. The luminescence properties of the crystals and their dependence on the type of anion as well as the length and oddity of the organic cation are described in detail. The obtained data expand our knowledge of the relationship between the structure of the organic cation, including its parity and structure, and the electronic and optical properties of the hybrid crystals.

1. Introduction

Hybrid perovskites, in which the A cation is an organic molecule, have been actively investigated since the late 2000s, when the prospect of their application in solar cells was revealed. Quite quickly, it became clear that by using sufficiently large organic cations whose sizes are larger than the limiting radius determined by the Goldschmidt tolerance factor, it is possible to obtain low-dimensional perovskites that exhibit new properties that are not inherent in three-dimensional structures.

One of the strategies for obtaining low-dimensional hybrid perovskites is the use of alkyl chains with ammonium groups at both ends as an organic cation. In this approach, the hydrogen of ammonium groups forms hydrogen bonds with halogens of $[MX_6]^{4-}$ (M – metal and X – halogen) octahedra,[1] providing structural integrity to the perovskite lattice with reduced dimensionality. The length of alkyl chains can also have a significant influence on the structural, optical, electronic and other properties of hybrid crystals. Several notable

studies[2–8] have recently been devoted to the investigation of the properties of various low-dimensional hybrid crystals with different alkyl chain lengths, as well as various B cations and anions.

The crystal structures of manganese chloride-based perovskites with 1,5-diaminopentane and 1,6-diaminohexane cations were investigated in ref. 4. According to the study, the diaminohexane chains possess an all-*trans* conformation, whereas the diaminopentanes have mixed *cis/trans* conformations.

The phenomena of reverse thermochromism and ferromagnetism as well as temperature-dependent electric conductance were studied in the 2D hybrid hexamethylenediamine copper chloride perovskite.[5] The structural analysis performed revealed that the organic cations are oriented in such a way as to form strong hydrogen bonds with the chlorines of the $CuCl_6$ octahedra. The authors showed that the presence of the hydrogen bonds reduces the effective charges of the chlorines, thereby diminishing the inter-octahedra repulsion. The latter leads to overall structure stabilization and affects the orientation and conformation of the organic cations. However, the details of the organic cation conformation were not reported. The optical properties of perovskites were studied by analyzing the transmission spectra of their thin films. The transmission spectra were transformed into absorption spectra, which demonstrated peaks at 313 nm and 385 nm. According to the authors, they are due to the ligand-to-metal charge transfer. The optical bandgap determined using the Tauc method was 2.78 eV.

The structural, optical, and electronic properties of $(NH_3C_3H_6NH_3)CuBr_4$ featuring rather a short carbon chain –

[a]Department of Materials Science, Shenzhen MSU-BIT University, PRC; Institute of High Technologies and Advanced Materials of the Far Eastern Federal University, Vladivostok, Russia
[b]Saint-Petersburg State University, Laboratory 'Photonics of Crystals', St.-Petersburg, Russia
[c]Shenzhen MSU-BIT University, PRC, Institute of High Technologies and Advanced Materials of the Far Eastern Federal University, Vladivostok, Russia.
E-mail: shtarev@mail.ru

1,3-diaminopropane – was studied in ref. 6. The optical bandgap determined by the authors utilizing the Tauc method was equal to 1.71 eV. In contrast to other reports, in this study, the authors used the XPS technique in order to estimate the potential of a valence band top. Additionally, the feasibility of perovskite practical applications was assessed by demonstrating its superior temperature, humidity, and UV irradiation resistance. Besides, the Seebeck coefficient of 13.8 μV K^{-1} and the power factor of 1.70 μW mK^{-2} measured at room temperature make this perovskite a potential n-type thermoelectric material.

A large set of hybrid 2D perovskites [H$_3$N-(CH$_2$)$_n$-NH$_3$]MX$_4$, (M = Cd, Mn, Pb, Cu, and Pd, and X = Cl and Br) with n varying in the range from 1 to 12 was investigated in ref. 7. Among other issues, the work focuses on conformational changes in the organic cations and the corresponding phase transitions. The authors used several experimental techniques including single crystal and powder XRD, differential scanning calorimetry, and IR spectroscopy. For instance, it was shown that the diaminobutane cation may have different molecular conformations (ttt, ttg, and gtg′), while diaminohexanes (M = Pb and Pd) coexist in two different molecular conformations. Unfortunately, the authors have focused only on the structure of the perovskites, elucidating neither their electronic nor optical properties.

The structural and optical properties of low-dimensional hybrid diaminohexane-based lead halogenides were studied in ref. 8. Therein, only the bromide and iodide crystals were sufficiently large in size. Since the bromide quality was rather poor, the only data that we found reliable were those of the iodide. The XRD studies conducted on the iodide showed that it is in fact a 2D material whose PbI$_6$ octahedra are separated by diaminohexane layers. Notably, within its structure, diaminohexane cations adopt an "extended form", *i.e.*, they bond neighboring inorganic layers through hydrogen bonds between -NH$_3$ groups and iodide anions. The second part of the work deals with the perovskite optical properties. The optical absorption spectra of the perovskite thin films reveal excitonic absorption peaks at 482 nm (2.57 eV), 390 nm (3.18 eV), and 332 nm (3.73 eV) for the iodide, bromide, and chloride, respectively. Knowing the perovskite bandgaps (I: E_g = 2.726 eV; Br: E_g = 3.346 eV; and Cl: E_g = 3.940 eV) and assuming that they are energetically close to the excitonic absorption bands, the exciton binding energies E_b can be estimated as E_b = E_g − $E_{(\text{exc. peak})}$, resulting in E_b = 153.3 meV, E_b = 166.4 meV, and E_b = 205.4 meV for the iodide, bromide, and chloride, respectively. Thus, there is a clear correlation between E_g and the type of perovskite anion.

In ref. 9, the structures of several low-dimensional hybrid perovskites of the diamine series with the general formula [H$_3$N-(CH$_2$)$_n$-NH$_3$]PbX$_4$, namely, bromine perovskites (X = Br) with 2, 4, and 10 carbon atoms (n = 2, 4, and 10), and iodine perovskites (X = I) with n = 4, 7, 8, and 12, are investigated. It was found that even alkyl chains with ammonium groups at both ends (n = 4, 8, 10, and 12) form layered (two-dimensional) hybrid perovskite structures, regardless of the anion (X = Br

and I). In this case, hydrogen atoms at both ends of the organic cations form hydrogen bonds with the halides of the inorganic layers. If the organic cation consists of a short even carbon chain (n = 2), the authors[9] also predict the formation of a two-dimensional perovskite, although they admit that in practice they observe one-dimensional ribbons consisting of corner-sharing PbBr$_6$ octahedra, which are structurally closely related to each other. That is, some transitional cases between 2-D and 1-D structures are observed. Odd alkyl chains behave differently. In ref. 9, only the compound [H$_3$N-(CH$_2$)$_7$-NH$_3$] PbI$_4$, which forms a zero-dimensional (0-D) perovskite with isolated octahedra of lead iodide [PbI$_6$] surrounded by [H$_3$N-(CH$_2$)$_7$-NH$_3$]$^{2+}$ cations, is referred to as such. The same team in a brief report[10] showed that when using as an organic cation five-membered alkyl chain with ammonium groups at both ends – [H$_3$N-(CH$_2$)$_5$-NH$_3$]$^{2+}$ – a one-dimensional perovskite is formed, in which the chains of octahedra [PbI$_6$] are oriented in the direction [111]. Thus, combining the results presented in ref. 7–11, it can be assumed that there is a relationship between the structure of the organic cation (in particular, the parity and length of the alkyl chain with ammonium groups at both ends) and the dimensionality of the corresponding perovskite. However, due to the fragmentary nature of the results presented in ref. 7–11, such a dependence has not been clearly formulated to date.

In ref. 11, the structure and phase transitions of another representative of hybrid perovskites, in which the organic cation is represented by an even alkyl chain with ammonium groups at both ends, are discussed – the composition is [H$_3$N-(CH$_2$)$_4$-NH$_3$]PbCl$_4$. This crystal has a two-dimensional structure (in full agreement with ref. 9) with the traditional orientation of organic and inorganic subsystems – inorganic layers of corner-sharing PbCl$_6$ octahedra are separated by layers of the organic cation; at the same time, the organic cation is oriented in such a way that the hydrogen of ammonium groups forms hydrogen bonds with chlorine. In this work, the authors have investigated and explained in detail the phase transition observed at 323.8 K. In the low-temperature phase (at room temperature), the PbCl$_6$ octahedra are deformed, the lead is displaced from the center, and the [H$_3$N-(CH$_2$)$_4$-NH$_3$]$^{2+}$ organic chain is not centrosymmetric and has a left-handed conformation at one end. The high temperature phase is characterized by a decrease in the unit cell parameter c from 1.9761 to 1.1011 nm and an increase in the angle β = 94.840 to 102.220. These changes are attributed by the authors[11] to the fact that the organic cation becomes symmetric as the temperature increases.

Another important study in the field under investigation is devoted to the study of the nature of broadband luminescence and its relationship with the structure using the example of a wide range of hybrid perovskites with differently structured organic cations.[12] In the current discourse, this article is important in that it describes two hybrid bromine perovskites, in which the organic cation is represented by four- and eight-membered alkyl chains with two amine groups at the ends – [H$_3$N-(CH$_2$)$_4$-NH$_3$]PbBr$_4$ and [H$_3$N-(CH$_2$)$_8$-NH$_3$]PbBr$_4$. In

addition to describing the unit cell of these perovskites, the work also describes their luminescence properties for the first time. In particular, the work suggests how the broad- and narrow-band luminescence of hybrid perovskites is related to the degree of disorder of inorganic octahedra in their structure. However, the analysis in this work was carried out on a sufficiently large sample of organic molecules, despite their heterogeneous structure.

In ref. 13, we investigated the structural, electronic, and optical properties of a number of hybrid crystals based on lead halides and hexamethylenediamine. In terms of data on the structure of the investigated class of hybrid crystals, this work supplements the studies of ref. 8 with data on the unit cell of chlorine crystals, since the authors of ref. 8 directly indicate that they failed to grow chlorine single crystals of sufficient quality for structural studies. In addition to the determination of the crystal structure of the chlorine crystal, this paper shows that the increase in the width of the bandgap in the series of crystals I → Br → Cl is due to the electronegativity of the anion and is accompanied by a decrease in the potential of the top of the valence band, while the potential of the bottom of the conduction band does not change.

In our other work,[14] we investigated the regularities of structural and optical properties depending on the halogen in hybrid crystals based on lead halides and 1,5-pentanediamine. This work complements the data on the unit cell structure of a number of hybrid crystals based on 1,5-pentanediamine, since earlier in ref. 10 the structure of only the iodine crystal was described. Besides the first description of the crystal structure of chlorine and bromine crystals in this paper, it is shown that the halogen anions determine the degree of octahedra distortion and the overall disorder of the perovskite crystal lattices. Also using IR spectroscopy methods, the interaction of amino groups of the organic cation and halogens of the inorganic subsystem during the formation of the crystal lattice is ana-

lyzed and it is shown that an optimal perovskite structure explores all of the above-mentioned possibilities. One of the manifestations of such a structure is the formation of as many N–H⋯X H bonds as possible.

In Table 1 are summarized the known data on various hybrid crystals based on lead halides, in which the organic cation is represented by an alkyl chain with ammonium groups at both ends. It can be seen that the delineated range of hybrid crystals has not been fully investigated. Thus, the structures of chlorine and bromine crystals have not been determined for sufficiently large organic cations. Optical properties have also been investigated rather fragmentarily. In this paper, we fill the gaps in the existing knowledge of hybrid perovskites, in which the organic cation is represented by an alkyl chain containing 4 to 8 carbon atoms and with ammonium groups at both ends. In particular, we investigate how the anion as well as the length and oddity of the organic cation affect their structural, optical, electronic and luminescence properties.

2. Experimental techniques and computational methods

2.1. Synthesis

Materials. Lead(II) bromide (PbBr$_2$, 98%, Acros Organics), lead(II) iodide (PbI$_2$, 99%, Acros Organics), lead(II) chloride (PbCl$_2$, 99%, Acros Organics), hydroiodic acid (HI, 56% in water, Iodobrom), hydrobromic acid (HBr, 48% in water, Iodobrom), hydrochloric acid (HCl, 36% in water, NevaReaktiv), 1,4-diaminobutane ((C$_4$)DA) (C$_4$H$_{12}$N$_2$, 98%, Macklin), 1,5-diaminopentane ((C$_5$)DA) (C$_5$H$_{14}$N$_2$, 98%, Macklin), 1,6-diaminohexane ((C$_6$)DA) (C$_6$H$_{16}$N$_2$, 99.5%, Acros Organics), 1,7-diaminoheptane ((C$_7$)DA) (C$_7$H$_{18}$N$_2$, 98%, Macklin), and 1,8-diaminooctane ((C$_8$)DA) (C$_8$H$_{20}$N$_2$, 98%,

Table 1 Known data on various hybrid crystals of the [H$_3$N-(CH$_2$)$_n$-NH$_3$]PbX$_4$ (X = Cl, Br, and I) type (further denoted as (C$_n$)DAPbX$_4$)

Compound	X = Cl	X = Br	X = I
(C$_4$)DAPbX$_4$	Ref. 11: parameters of the unit cell and atomic positions were determined, and the phase transition was detected	Ref. 9: parameters of the unit cell and atomic positions were determined Ref. 12: luminescence properties are described	Ref. 9: parameters of the unit cell and atomic positions were determined
(C$_5$)DAPbX$_4$	Ref. 14: parameters of the unit cell and atomic positions, as well as the optical width of the bandgap were determined and the luminescence was described	Ref. 14: parameters of the unit cell and atomic positions, as well as the optical width of the bandgap were determined and the luminescence was described	Ref. 10: parameters of the unit cell and atomic positions were determined Ref. 14: optical width of the bandgap was determined and the luminescence was described
(C$_6$)DAPbX$_4$	Ref. 13: parameters of the unit cell and atomic positions, as well as optical widths of the bandgap were determined	Ref. 8: parameters of the unit cell and atomic positions, as well as optical widths of the bandgap were determined	Ref. 8: parameters of the unit cell and atomic positions, as well as optical widths of the bandgap were determined
(C$_7$)DAPbX$_4$	—	—	Ref. 9: parameters of the unit cell and atomic positions were determined
(C$_8$)DAPbX$_4$	—	Ref. 12: parameters of the unit cell and atomic positions were determined, luminescence properties were described	Ref. 9: parameters of the unit cell and atomic positions were determined

Macklin) were purchased and used in this work. All reagents were used as received without further purification.

Synthesis 1 of [H₃N-(CH₂)₄-NH₃]PbI₄ further denoted as (C₄) DAPbI₄. PbI₂ (2.00 g; 4.34 mmol) was dissolved in HI (9 ml) and (C₄)DA (0.38 g; 4.34 mmol) was separately dissolved in HI (9 ml). Then the resulting solutions were mixed, and a precipitate formed after a few minutes. The reaction mixture was heated until complete dissolution of the precipitate and then cooled slowly to room temperature. The obtained crystals were filtered, washed with acid (HI) and acetone and then dried in a vacuum oven at 50 °C.

Synthesis 2 of [H₃N-(CH₂)₄-NH₃]PbBr₄ further denoted as (C₄)DAPbBr₄. PbBr₂ (2.00 g; 5.45 mmol) was dissolved in HBr (9 ml) and (C₄)DA (0.48 g; 5.45 mmol) was separately dissolved in HBr (9 ml). The synthesis process then follows synthesis **1**.

Synthesis 3 of [H₃N-(CH₂)₄-NH₃]PbCl₄ further denoted as (C₄)DAPbCl₄. PbCl₂ (2.00 g; 7.19 mmol) was dissolved in HCl (47 ml) and (C₄)DA (0.63 g; 7.19 mmol) was separately dissolved in HCl (9 ml). Then the resulting solutions were mixed, and a crystalline precipitate formed after a few days. The obtained crystals were filtered, washed with acid (HCl) and acetone and then dried in a vacuum oven at 50 °C.

Synthesis 4 of [H₃N-(CH₂)₅-NH₃]PbI₄ further denoted as (C₅) DAPbI₄. PbI₂ (2.00 g; 4.34 mmol) was dissolved in HI (9 ml) and (C₅)DA (0.44 g; 4.34 mmol) was separately dissolved in HI (9 ml). The synthesis process then follows synthesis **1**.

Synthesis 5 of [H₃N-(CH₂)₅-NH₃]PbBr₄ further denoted as (C₅)DAPbBr₄. PbBr₂ (2.00 g; 5.45 mmol) was dissolved in HBr (9 ml) and (C₅)DA (0.56 g; 5.45 mmol) was separately dissolved in HBr (9 ml). The synthesis process then follows synthesis **1**.

Synthesis 6 of [H₃N-(CH₂)₅-NH₃]PbCl₄ further denoted as (C₅)DAPbCl₄. PbCl₂ (2.00 g; 7.19 mmol) was dissolved in HCl (47 ml) and (C₅)DA (0.73 g; 7.19 mmol) was separately dissolved in HCl (9 ml). The synthesis process then follows synthesis **3**.

Synthesis 7 of [H₃N-(CH₂)₆-NH₃]PbI₄ further denoted as (C₆) DAPbI₄. PbI₂ (2.00 g; 4.34 mmol) was dissolved in HI (9 ml) and (C₆)DA (0.50 g; 4.34 mmol) was separately dissolved in HI (9 ml). The synthesis process then follows synthesis **1**.

Synthesis 8 of [H₃N-(CH₂)₆-NH₃]PbBr₄ further denoted as (C₆)DAPbBr₄. PbBr₂ (2.00 g; 5.45 mmol) was dissolved in HBr (9 ml) and (C₆)DA (0.63 g; 5.45 mmol) was separately dissolved in HBr (9 ml). The synthesis process then follows synthesis **1**.

Synthesis 9 of [H₃N-(CH₂)₆-NH₃]PbCl₄ further denoted as (C₆)DAPbCl₄. PbCl₂ (2.00 g; 7.19 mmol) was dissolved in HCl (47 ml) and (C₆)DA (0.83 g; 7.19 mmol) was separately dissolved in HCl (9 ml). The synthesis process then follows synthesis **3**.

Synthesis 10 of [H₃N-(CH₂)₇-NH₃]PbI₄ further denoted as (C₇)DAPbI₄. PbI₂ (2.00 g; 4.34 mmol) was dissolved in HI (9 ml) and (C₇)DA (0.56 g; 4.34 mmol) was separately dissolved in HI (9 ml). The synthesis process then follows synthesis **1**.

Synthesis 11 of [H₃N-(CH₂)₇-NH₃]PbBr₄ further denoted as (C₇)DAPbBr₄. PbBr₂ (2.00 g; 5.45 mmol) was dissolved in HBr (9 ml) and (C₇)DA (0.71 g; 5.45 mmol) was separately dissolved in HBr (9 ml). The synthesis process then follows synthesis **1**.

Synthesis 12 of [H₃N-(CH₂)₇-NH₃]PbCl₄ further denoted as (C₇)DAPbCl₄. PbCl₂ (2.00 g; 7.19 mmol) was dissolved in HCl (47 ml) and (C₇)DA (0.94 g; 7.19 mmol) was separately dissolved in HCl (9 ml). The synthesis process then follows synthesis **3**.

Synthesis 13 of [H₃N-(CH₂)₈-NH₃]PbI₄ further denoted as (C₈)DAPbI₄. PbI₂ (2.00 g; 4.34 mmol) was dissolved in HI (9 ml) and (C₈)DA (0.62 g; 4.34 mmol) was separately dissolved in HI (9 ml). The synthesis process then follows synthesis **1**.

Synthesis 14 of [H₃N-(CH₂)₈-NH₃]PbBr₄ further denoted as (C₈)DAPbBr₄. PbBr₂ (2.00 g; 5.45 mmol) was dissolved in HBr (9 ml) and (C₈)DA (0.78 g; 5.45 mmol) was separately dissolved in HBr (9 ml). The synthesis process then follows synthesis **1**.

Synthesis 15 of [H₃N-(CH₂)₈-NH₃]PbCl₄ further denoted as (C₈)DAPbCl₄. PbCl₂ (2.00 g; 7.19 mmol) was dissolved in HCl (47 ml) and (C₈)DA (1.04 g; 7.19 mmol) was separately dissolved in HCl (9 ml). The synthesis process then follows synthesis **1**.

2.2. Characterization

The powder diffraction data of (C_n)DAPbX₄ (n = 4–8 and X = Cl, Br, and I) were collected at room temperature (25 °C) with a Colibri powder diffractometer (Bourevestnik, Russia) with Cu-Kα radiation and a linear Muthen2 detector. The step size of 2θ was 0.02° and the counting time was 35.4 s per step.

The full profile X-ray analysis of (C_7)DAPbCl₄ (a) and (C_8) DAPbCl₄ single crystals was performed using a Bruker Kappa Apex II diffractometer with graphite-monochromatized MoK_α radiation[15] at 100 K. The data reduction and multi-scan absorption correction were carried out using the manufacturer's software.

The optical properties of the investigated samples were studied by diffuse reflectance spectroscopy. Diffuse reflectance spectra in the form $A(\lambda) = 1 - R(\lambda)$, where A – absorption coefficient, R – reflection coefficient, and λ – wavelength of radiation, were recorded in the spectral range from 250 to 800 nm at room temperature (25 °C) using a PerkinElmer Lambda 950 UV-Vis-NIR spectrophotometer (UK), equipped with an integrating sphere of 150 mm. Spectralon was used as a reference standard.

The low-temperature luminescence spectra and luminescence excitation spectra of the hybrid crystal samples in the spectral range 250–800 nm were recorded using an FL 8500 PerkinElmer fluorescence spectrometer. All the recordings were performed at a temperature of 77 K (−196 °C) using the Low Temperature Cell Holder from PerkinElmer.

2.3. Computational approach

The electronic structures of (C_n)DAPbX₄ were modeled using the periodic DFT approach. The geometry of the structures was not optimized for these studies, and all calculations were performed based on the geometry of crystals obtained during the experiments. This was accomplished employing the Projector-Augmented-Wave (PAW) approach[16] in conjunction with the

PBE[17,18] density functional, within the GGA approach, as implemented in the VASP 5.4.4 program.[19–22] The SCF energy convergence criterion was set to 1.0×10^{-7} eV. Atomic kinetic energy cutoffs were set to their default values. Brillouin Zones (BZs) were sampled over a Monkhorst–Pack grid[23] of $7 \times 9 \times 9$ k-points ($9 \times 9 \times 3$ k-points for the monocrystalline chloride). Electronic band structures were computed at 181 k-points along the Γ-A-C-D-D1-E-X-Y-Y1-Z high symmetry path of the monoclinic BZ. The electronic band structures and density of states were plotted using the Gnuplot 5.2 software package.[24] Throughout the text, chemical structures are visualized using the program VESTA.[25]

3. Results

3.1. Powder X-ray diffraction

It was shown above (see Table 1) that for some of the hybrid crystals under study, the crystal structures were investigated earlier. Therefore, the powder X-ray diffraction (PXRD) analysis method was used to confirm the formation of the target phase and its phase homogeneity. Fig. S1–S15† show the experimental PXRD patterns of these hybrid crystals in comparison with the calculated PXRD patterns obtained from known structures. The unit cells for this purpose were taken from the open crystallographic database[26] or other sources (see ref. 27 and references therein).

One can see excellent agreement between the calculated PXRD patterns and the experimental ones for all the samples considered. That is, we can state that in all cases the formation of hybrid crystals occurred, the unit cells of which are identical to those described earlier.

For the crystal $(C_7)DAPbBr_4$, for which the structure was not established either previously or in the present study due to the inability to grow this crystal in a single crystal form, the PXRD patterns are still characteristic and suggest that these crystals are formed two-dimensionally.

3.2. Single-crystal X-ray diffraction

For those samples of hybrid crystals for which the structures have not been previously described, the method of single-crystal X-ray diffraction was applied. Fig. 1 shows the unit cells of the new structures first described in this study. The crystal structures of the compounds can be obtained from the Cambridge Crystallographic Data Center by quoting the depository numbers CCDC – 2362771 $((C_7)DAPbCl_4)$ and CCDC – 2362165 $((C_8)DAPbCl_4)$.

The data obtained indicate that all the hybrid crystals studied by single-crystal XRD are two-dimensional with planes of corner-sharing $PbCl_6$ octahedra, between which are located diamine molecules oriented by NH_3 groups towards the inorganic planes.

3.3. Band structures

To complement the above schematic picture of the perovskite band structures, DFT PBE modeling of their electronic structures was performed. Fig. 2 shows the calculated band structure and density of states for the $(C_4)DAPbCl_4$ hybrid crystal.

The calculations show that this hybrid crystal is a direct-band semiconductor and the transition from the valence band
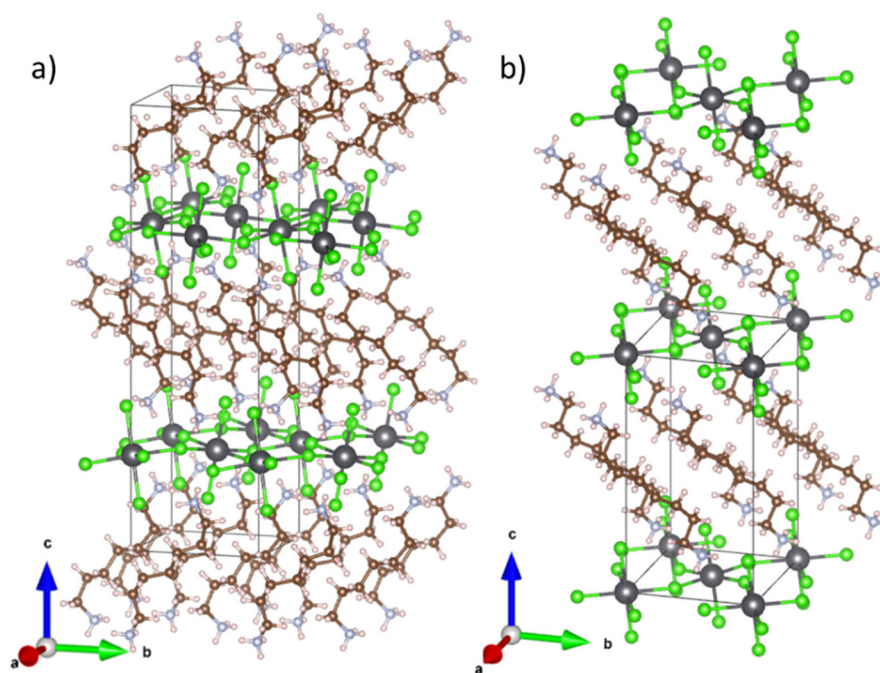

Fig. 1 Ball-and-stick models of the unit cells of $(C_7)DAPbCl_4$ (a) and $(C_8)DAPbCl_4$ (b) hybrid crystals: gray balls are lead atoms, green – chlorine atoms, brown – carbon atoms, light gray – nitrogen atoms, and light brown – hydrogen atoms.
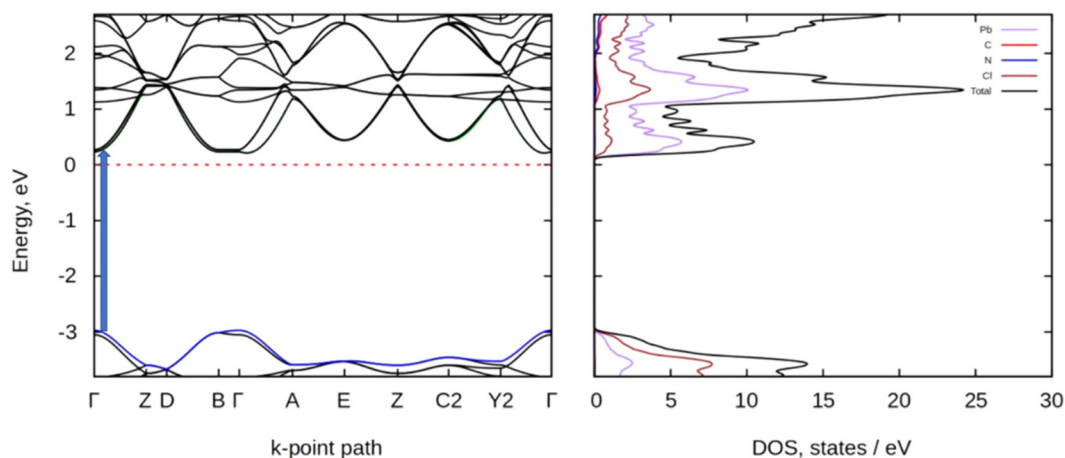
Fig. 2 Electronic band structure (left) and density of states (right) for a $(C_4)DAPbCl_4$ hybrid crystal. The blue arrow indicates the transition between the top of the valence band and the bottom of the conduction band.

to the conduction band occurs at the point Γ of the Brillouin zone. In this case, the width of the bandgap according to calculations is about 3 eV.

If we turn to the analysis of the density of states (right part of Fig. 2), we can see that there are three regions in the conduction band, in which the density of states is maximum. The first region forms the bottom of the conduction band and consists mainly of the electron orbitals of the B (lead) cation. The transitions of electrons into this region from the top of the valence band form the fundamental absorption edge and correspond to the optical width of the bandgap, denoted as $E_g(I)$. The second and third regions – denoted as $E_g(II)$ and $E_g(III)$ – start at about 1 eV and 2 eV above the first one. It also consists mainly of lead orbitals. Their significance will be explained later.

For the other studied hybrid crystal, for which similar calculations were also performed (Fig. S18–S27† and Fig. 3), it follows that chlorine and bromine perovskites are direct-band

semiconductors with the transition Γ → Γ regardless of the oddity of the alkyl chain of their organic cation. For iodine crystals, the situation is different: crystals with the even alkyl chain NH_3-$(CH_2)_n$-NH_3 (n = 4, 6, and 8) are direct-band semiconductors, whereas those with the odd chain (n = 5 and 7) are indirect-band semiconductors.

3.4. Diffuse reflectance spectroscopy

Diffuse reflectance spectroscopy was used to determine the optical bandgap. This is a common method for powder samples, but it tends to underestimate the fundamental bandgap energy, which should be determined from optical absorption from single crystals (which is not possible in this study).[28] The diffuse reflectance spectra of $(C_n)DAPbX_4$ are demonstrated in Fig. 4. All the above spectra have several common features, despite their significantly different compositions. First, the intrinsic absorption region of chlorine crystals is maximally shifted to the blue region, and that of iodine crys-
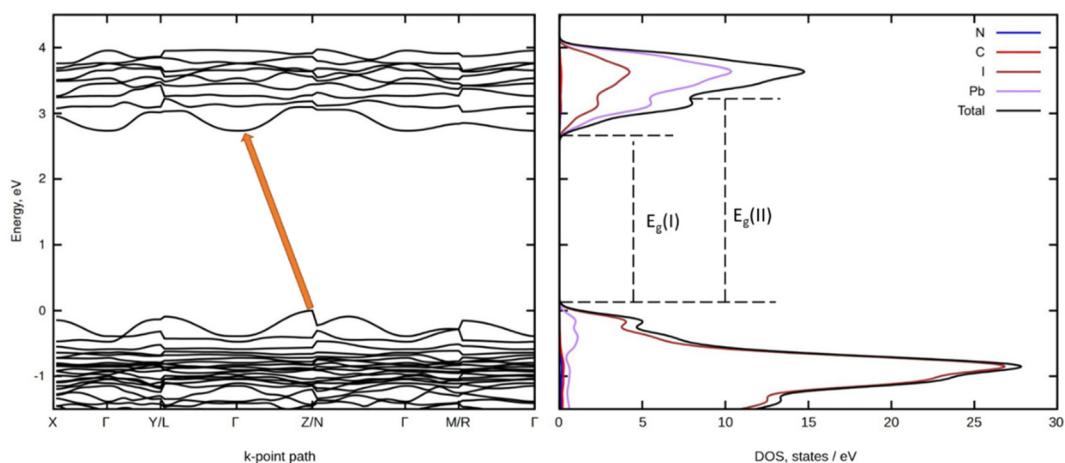
Fig. 3 Electronic band structure (left) and density of states (right) for a $(C_5)DAPbI_4$ hybrid crystal. The blue arrow indicates the transition between the top of the valence band and the bottom of the conduction band.
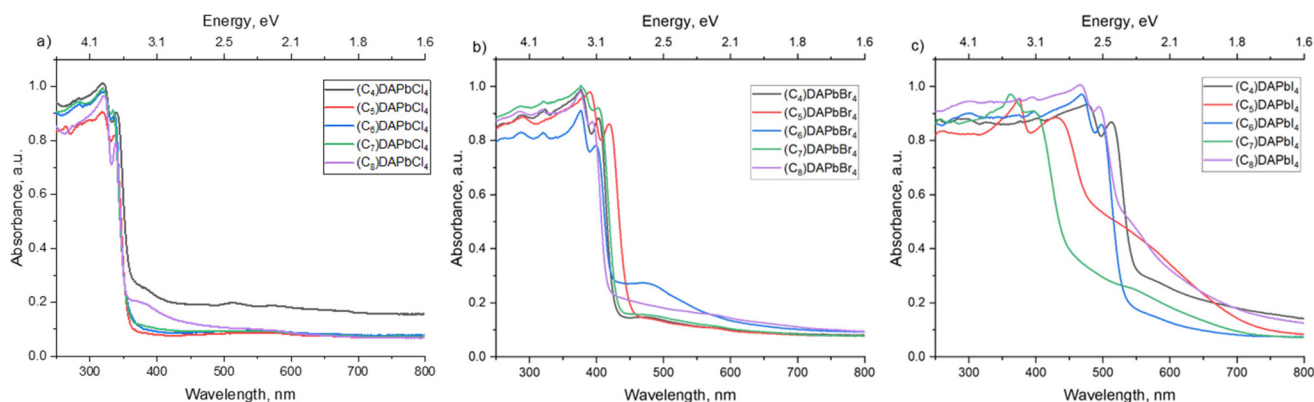
Fig. 4 Diffuse reflectance spectra of $(C_n)DAPbCl_4$ (a), $(C_n)DAPbBr_4$ (b), and $(C_n)DAPbI_4$ (c).

tals to the red region, with bromine crystals occupying an intermediate position. Secondly, local absorption maxima are present in the intrinsic absorption region for all investigated samples. From the differences presented in Fig. 4, it is necessary to point out the significant absorption in the non-intrinsic region, which is inherent in all iodine crystals.

The derivative method[29] was used to determine the bandgap width of the hybrid crystals analyzed in this work (Fig. 5). On the curves shown, two maxima are characteristic of all hybrid crystals studied in this work. The position of the lower-energy maximum corresponds to the optical width of the bandgap of crystals, and the second maximum, shifted to the region of higher energies, is obviously related to the absorption bands described above in the region of their fundamental absorption and to the second maxima of the densities of states discussed in section 3.3.

For the convenience of analyzing the obtained results, they are presented in Fig. 6 and Table 2. In this figure and in the table, the optical bandgap is denoted as $E_g(I)$, and the energy corresponding to the second maximum in Fig. 5 is denoted as $E_g(II)$. The experimentally obtained values of the energies of the bandgap agree well with the DFT modeling data; they are somewhat smaller than the experimentally obtained values,
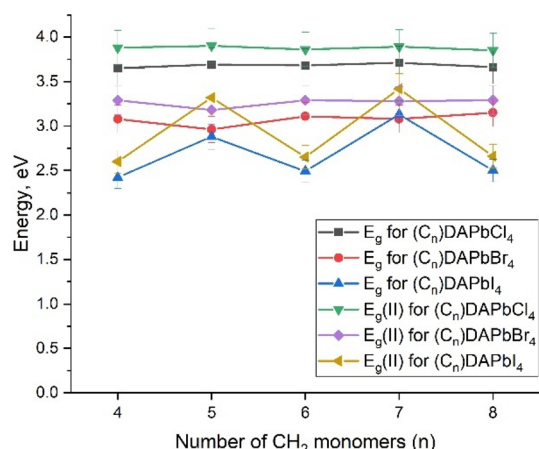

Fig. 6 Dependence of the bandgap of $(C_n)DAPbX_4$ (X = Cl, Br, and I) on the number of CH_2 monomers in the organic cation structure.

but this underestimation is common for the pseudopotentials used.[30]

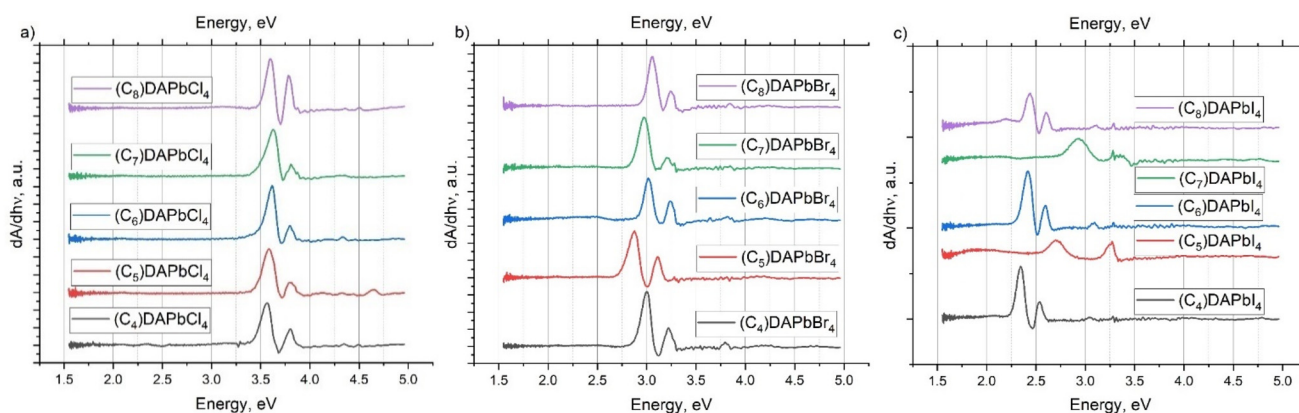Regularities in the dependence of the optical width of the bandgap $E_g(I)$ on both the length of the carbon chain of the

Fig. 5 Approximation by the method of derivatives of $(C_n)DAPbCl_4$ (a), $(C_n)DAPbBr_4$ (b), and $(C_n)DAPbI_4$ (c).

Table 2 Bandgaps of $(C_n)DAPbX_4$ (X = Cl, Br, and I)

Compound	$E_g(I)$, eV			$E_g(II)$, eV		
	X = Cl	X = Br	X = I	X = Cl	X = Br	X = I
$(C_4)DAPbX_4$	3.57	3.00	2.35	3.8	3.22	2.54
$(C_5)DAPbX_4$	3.58	2.87	2.7	3.8	3.11	3.27
$(C_6)DAPbX_4$	3.61	3.02	2.41	3.8	3.24	2.6
$(C_7)DAPbX_4$	3.62	2.97	2.92	3.81	3.21	3.35
$(C_8)DAPbX_4$	3.59	3.05	2.44	3.8	3.25	2.6

organic cation and the anion are traced. For chloride hybrid crystals, $E_g(I)$ does not depend on the carbon chain length and is in the range of 3.57–3.62 eV. For bromine hybrid crystals, the $E_g(I)$ of "even" hybrid crystals (i.e., such crystals whose organic cation in the structure has an even number of CH_2 monomers, n = 4, 6, and 8) is in the range of 3–3.05 eV, whereas the $E_g(I)$ for "odd" hybrid crystals (n = 5 and 7) is slightly lower and is 2.87–2.97 eV. The most pronounced differences, caused by the oddity of the carbon chain of the organic cation, appear in iodine hybrid crystals.

As can be seen from Fig. 6, there is an increase in $E_g(I)$ as the length of the carbon chain (n) increases. And just as in the case of bromine perovskites, there is a modulation of $E_g(I)$ vibrations due to the oddity of the carbon chain. However, in this case, the situation is opposite to bromide hybrid crystals: for "even" crystals (n = 4, 6, and 8), we observe a monotonic increase in $E_g(I)$ from 2.35 eV to 2.44 eV, and for odd crystals (n = 5 and 7), the width of the bandgap is much higher and is 2.7 eV and 2.92 eV, respectively.

3.5. Low temperature photoluminescence

The low-temperature photoluminescence of hybrid crystals based on lead halides and a homologous series of diaminoalkanes of the form $(C_n)DAPbX_4$ (n = 4–8 and X = Cl, Br, and I) was investigated as a function of halogen and organic cation length. The corresponding emission spectra and luminescence excitation spectra obtained at 77 K are presented in Fig. 7–9.

• Broadband luminescence in the emission spectra;

Here it is necessary to establish terminological clarity regarding the terms that we will use further to describe the luminescence properties of the investigated materials. The free exciton (FE) is a delocalized exciton state. Its formation is manifested by a narrow band in the luminescence excitation spectrum with energy less than the bandgap. An self-trapped exciton (STE) is an exciton that polarizes the lattice, creating a local energy minimum, and as a result localizes in some region of the crystal. Usually, the energy change caused by lattice polarization is small and the energy shift of such exciton luminescence relative to the FE is also small. The difference between these two energies (E_{tr}) corresponds to the autolocalization energy of the free exciton (see the inset in Fig. 7–9):

$$E_{tr} = E_{ex} - E_{em}. \tag{1}$$

A defect-trapped exciton (DTE) is an exciton captured by a defect when one of the exciton components, an electron or a hole, is captured by the Coulomb field of the defect. Then the localization energy can be significant, resulting in a large shift of the luminescence of such an exciton with respect to the FE. Since there is a large variety of defects (both in type and energy) in a real crystal, their distribution sets a wide distribution of luminescence.[31] This is typical of any defect-related luminescence.

Fig. 7(a) shows the low temperature photoluminescence spectrum of the $(C_4)DAPbCl_4$ sample. The emission spectrum shows intense broadband luminescence with a maximum in the 553 nm region. Several bands can also be distinguished in the luminescence excitation spectrum. Thus, the luminescence is most effectively excited by radiation with a wavelength of 315 nm, but closer to the edge of intrinsic absorption, there are two more luminescence excitation bands with maxima at 333.2 and 341.6 nm. If we analyze the luminescence properties of the remaining chlorine-based hybrid crystals presented in Fig. 7(b–e), it can be stated that the case of $(C_4)DAPbCl_4$ is typical of the crystals of this series. All of them are characterized by the presence of the following.

narrow excitation bands in the photoluminescence excitation spectra. The photoluminescence spectra of bromine-based hybrid crystals, shown in Fig. 8, reveal both similarities with chlorine crystals and unique characteristic features. Thus, in the luminescence excitation spectra of bromine hybrid crystals, narrow luminescence excitation peaks are also present.

In contrast to chlorine samples, bromine crystals are characterized by the following features.

• The presence of two photoluminescence bands: narrow-band and broadband.

• Higher luminescence intensity of the STE compared to the DTE.

• Decrease in the ratio of luminescence intensities I_{STE}/I_{DTE} as the length of the organic cation increases from 105 for (C_4)DA to 1 for (C_8)DA.

• The value of the free exciton localization energy (E_{tr}) – from 20 to 31 meV.

The luminescence of iodine hybrid crystals presented in Fig. 9 differs significantly from those in the chlorine and bromine cases discussed earlier. The first significant difference is that the samples with an odd number of carbon atoms in the organic cation, $(C_5)DAPbI_4$ and $(C_7)DAPbI_4$, do not exhibit luminescence properties, which is obviously due to their one-dimensional structure. Secondly, the photoluminescence intensity of iodine samples is orders of magnitude lower than the usual values for chlorine and bromine.

Otherwise, the luminescence of samples with an even number of carbon atoms in the organic cation – $(C_4)DAPbI_4$, $(C_6)DAPbI_4$, and $(C_8)DAPbI_4$ – is similar to the luminescence of bromine samples: the intensity of narrow-band STE-luminescence is several times greater than the intensity of broadband
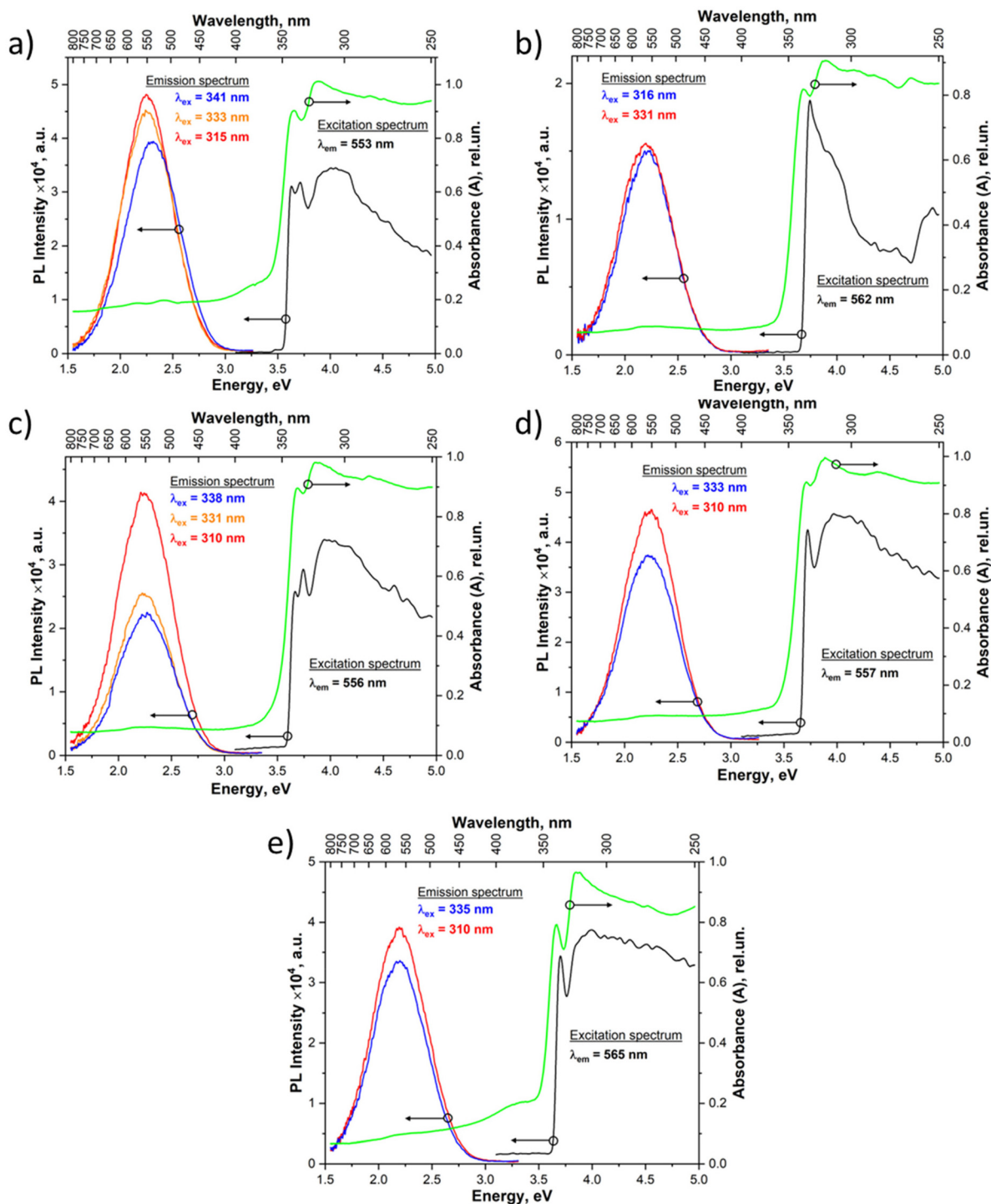
Paper

Dalton Transactions

Fig. 7 Low temperature (77 K) photoluminescence spectrum of $(C_n)DAPbCl_4$: $n = 4$ (a), $n = 5$ (b), $n = 6$ (c), $n = 7$ (d), and $n = 8$ (e).

DTE-luminescence, and the localization energy of free excitons E_{tr} lies in the range of 11–31 meV.

The presence of two luminescence bands at once makes it possible to analyze the ratio of intensities between them and conclude how the composition (the halogen, length and parity of the carbon chain of the organic cation) affects the

probability of radiative recombination from the state of the autolocalized exciton or its transition to the state of localization on the defect. Table 3 shows some low-temperature photoluminescence parameters for various hybrid crystals of the $(C_n)DAPbX_4$ type depending on their anionic (X = Cl, Br, and I) and cationic ($n = 4$–8) composition.
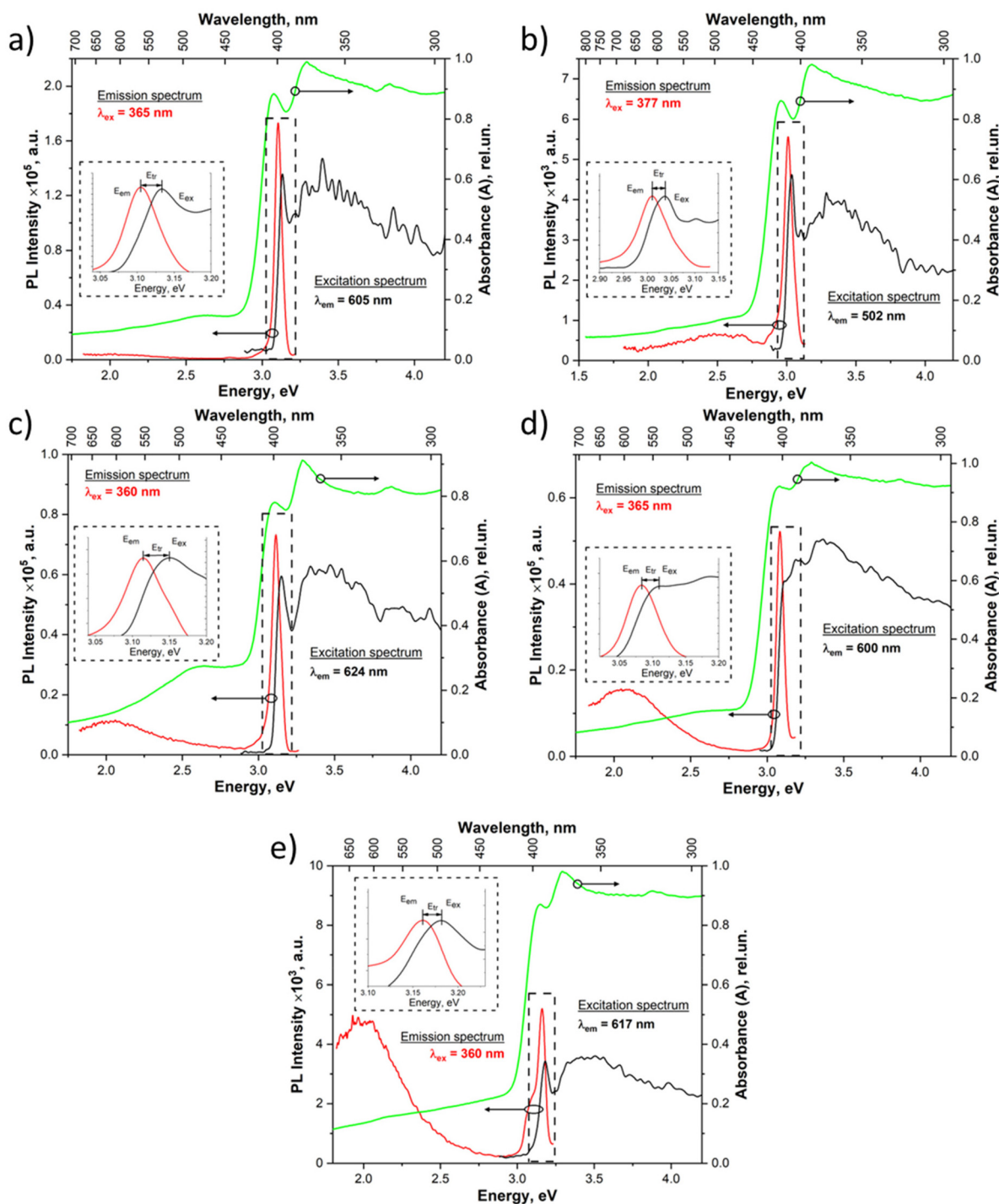
Fig. 8 Low-temperature (77 K) photoluminescence spectrum of $(C_n)DAPbBr_4$: $n = 4$ (a), $n = 5$ (b), $n = 6$ (c), $n = 7$ (d), and $n = 8$ (e). For clarity, the luminescence excitation spectrum for (a) has been multiplied by 40, for (b) by 6, and for (c) and (d) by 4. The insets show regions in the region of exciton absorption and the corresponding photoluminescence spectrum with intensities normalized with respect to each other.

4. Discussion

The data on the unit cell structure of hybrid crystals of different compositions known from the literature and obtained in the present study allow us to analyze how the halogen and the length of the organic cation affect various structural para-meters. Fig. 10–14 show the unit cells of all the hybrid crystals investigated. It can be seen that in all cases, two-dimensional crystals are formed except for $(C_5)DAPbI_4$ and $(C_7)DAPbI_4$. In these cases, one-dimensional structures are formed. Thus, the halogen and oddity of the alkyl diamine in the structure of hybrid crystals determine their dimensionality.
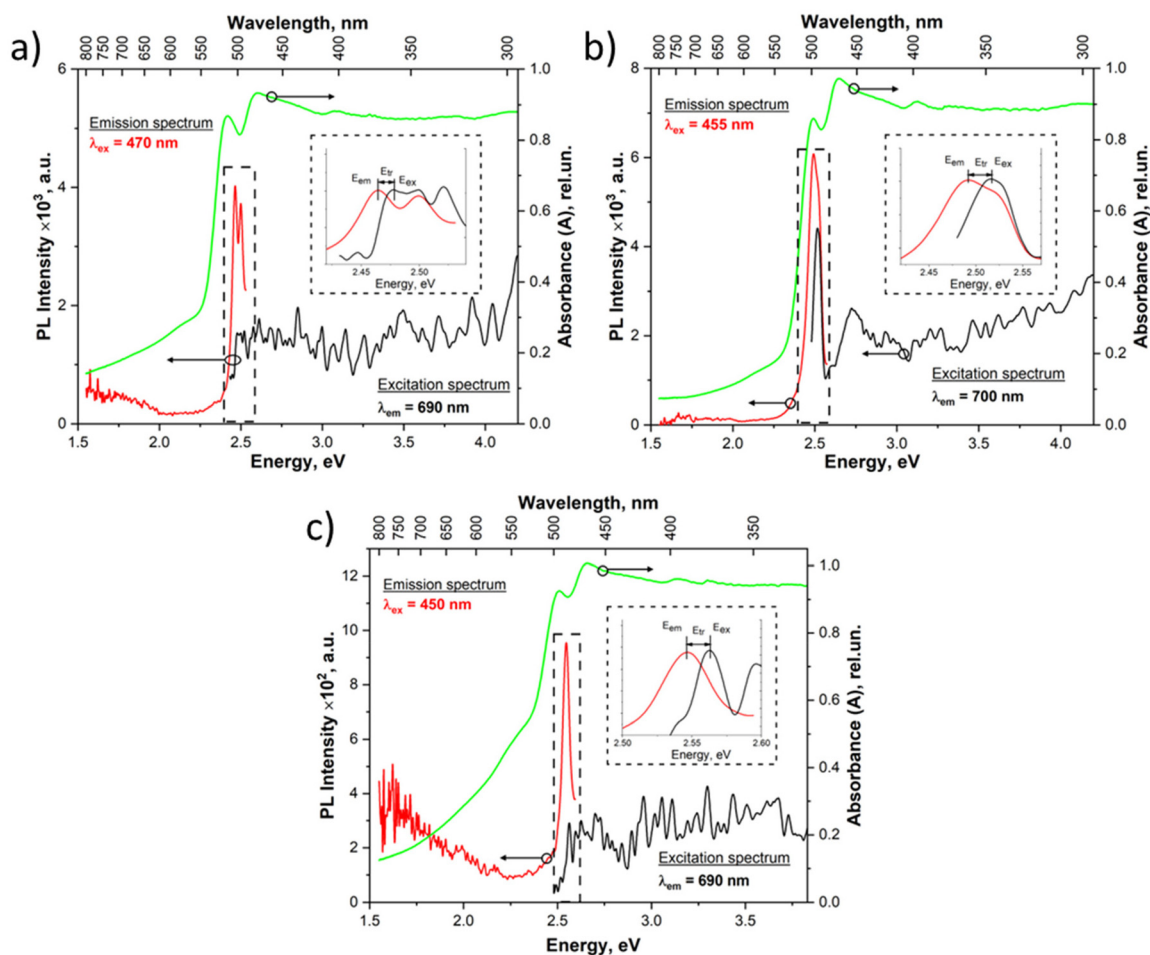
Fig. 9 Low-temperature (77 K) photoluminescence spectrum of (Cn)DAPbI4: *n* = 4 (a), *n* = 6 (b), and *n* = 8 (c). For clarity, the luminescence excitation spectrum for (a) and (b) has been multiplied by 5 and for (c) by 2. The insets show the areas in the region of exciton absorption and the corresponding photoluminescence spectrum with intensities normalized with respect to each other.

Table 3 Basic low-temperature (77 K) photoluminescence parameters of various hybrid crystals of the $(C_n)DAPbX_4$ type

Compound	E_{STE}, nm	E_{STE}, eV	E_{DTE}, nm	E_{DTE}, eV	E_{ex}, nm	E_{ex}, eV	E_{tr}, meV	I_{FE}/I_{STE}
$(C_4)DAPbCl_4$	No	No	550.0	2.254	341.6	3.63	—	—
$(C_5)DAPbCl_4$	No	No	564.9	2.195	331.7	3.738	—	—
$(C_6)DAPbCl_4$	No	No	550.0	2.254	339.5	3.652	—	—
$(C_7)DAPbCl_4$	No	No	552.5	2.244	333.1	3.723	—	—
$(C_8)DAPbCl_4$	No	No	562.2	2.206	334.2	3.71	—	—
$(C_4)DAPbBr_4$	399.3	3.105	443.9	2.793	395.6	3.134	29.0	105.482
$(C_5)DAPbBr_4$	412.1	3.009	498.6	2.487	408.2	3.038	28.7	11.161
$(C_6)DAPbBr_4$	398.2	3.114	619.3	2.002	394.2	3.146	31.6	7.136
$(C_7)DAPbBr_4$	402.1	3.084	598.2	2.073	398.9	3.108	24.7	3.362
$(C_8)DAPbBr_4$	392.4	3.16	624.6	1.985	389.9	3.18	20.3	1.106
$(C_4)DAPbI_4$	504.1	2.460	736.6	1.683	497.6	2.492	32.2	6.353
$(C_5)DAPbI_4$	No	No	No	No	No	No	—	—
$(C_6)DAPbI_4$	498.5	2.487	709.0	1.749	492.4	2.518	30.9	8.416
$(C_7)DAPbI_4$	No	No	No	No	No	No	—	—
$(C_8)DAPbI_4$	486.7	2.548	676.8	1.832	484.5	2.559	11.6	5.016

Notation for the table: "no" – luminescence is absent and "—" – inapplicability of this parameter.

The distance between the planes formed by the lead atoms of inorganic octahedra can be measured from the position of the main reflex of PXRD patterns. Fig. 15 shows how the distance between the inorganic layers varies with the amount of monomer in the organic cation for hybrid crystals based on different halogens.
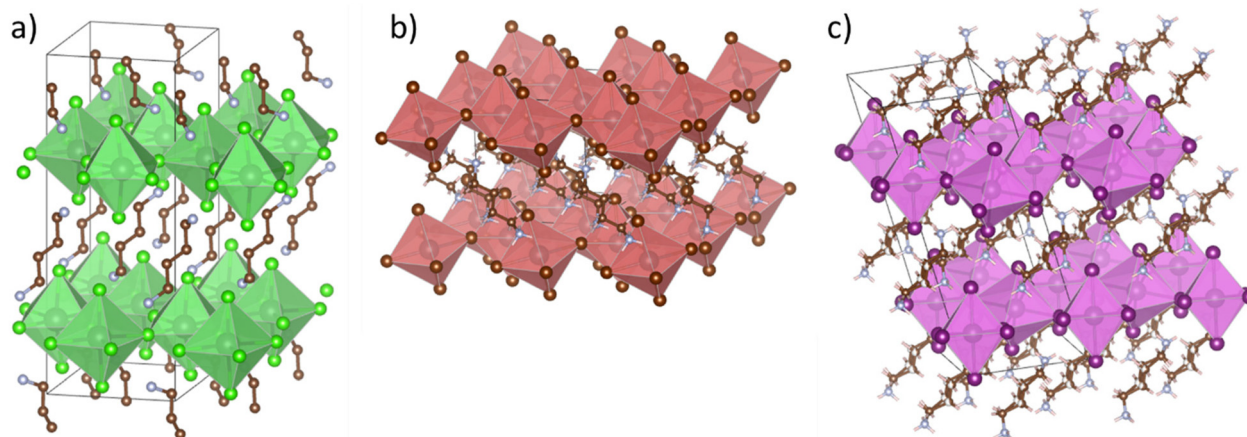
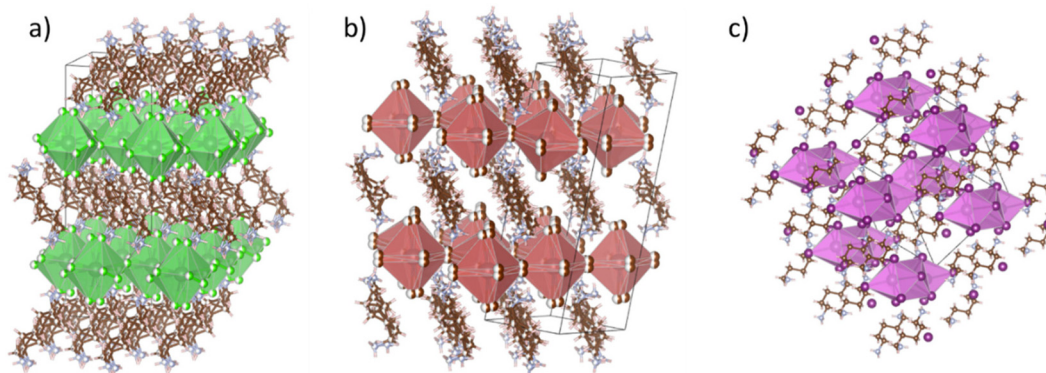**Fig. 10** Ball-and-stick models of (C_4)DAPbX$_4$ hybrid crystals: X = Cl (a), X = Br (b), and X = I (c).

Fig. 11 Ball-and-stick models of (C_5)DAPbX$_4$ hybrid crystals: X = Cl (a), X = Br (b), and X = I (c).
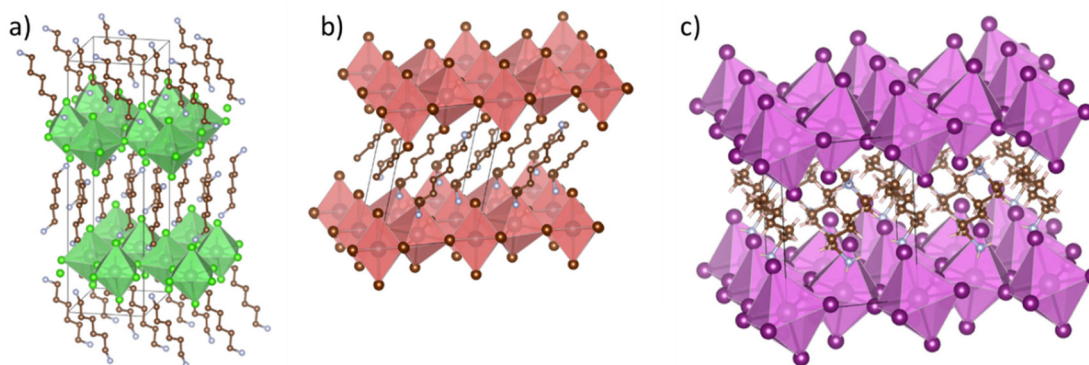

Fig. 12 Ball-and-stick models of (C_6)DAPbX$_4$ hybrid crystals: X = Cl (a), X = Br (b), and X = I (c).

It can be seen that as the length of the carbon skeleton of the organic cation increases, there is a proportional increase in the distance between the inorganic layers, and in the case of iodine crystals, this increase is slower than in the case of bromine or chlorine structures.

The structure of hybrid crystals largely determines their optical and electronic properties. Therefore, for the purposes of the present study, it is important to analyze how the anion and organic cation influence the emerging structure of hybrid crystals. Octahedra of two neighboring inorganic planes can be arranged parallel to each other without displacement, forming Dion–Jacobson (DJ) structures, or they can be displaced by $\frac{1}{2}$ of the octahedron width, forming Ruddlesden–Popper (RP) structures.
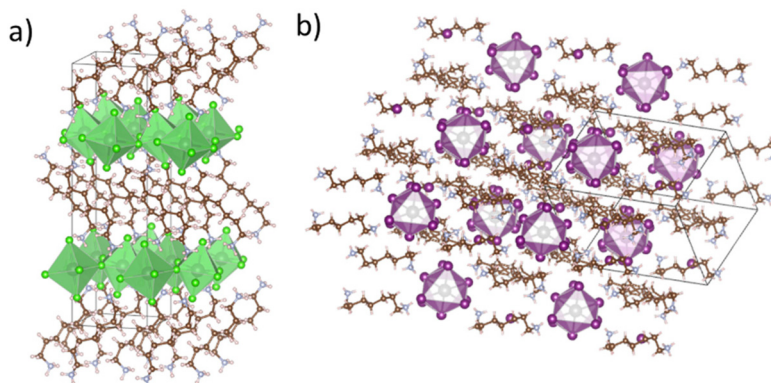
Fig. 13 Ball-and-stick models of $(C_7)DAPbX_4$ hybrid crystals: X = Cl (a) and X = I (b).
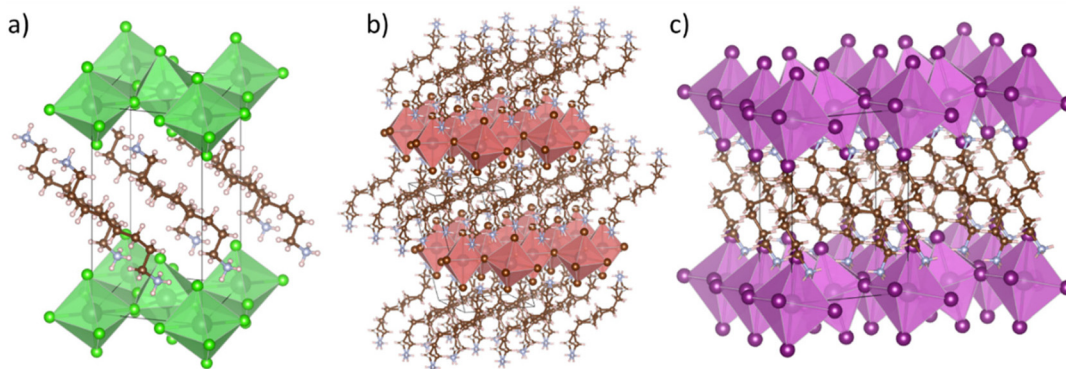

Fig. 14 Ball-and-stick models of $(C_8)DAPbX_4$ hybrid crystals: X = Cl (a), X = Br (b), and X = I (c).
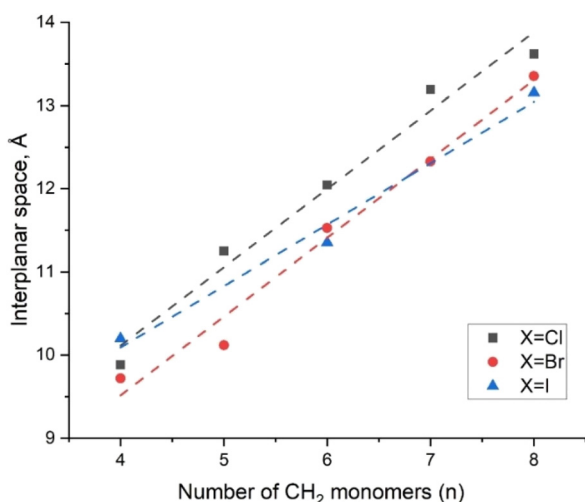

Fig. 15 Dependence of the distance between inorganic layers on the number of monomers in the organic cation.

If we analyze the structures of hybrid compounds based on lead halides and a homologous series of limiting diamines of the form $(C_n)DAPbX_4$ (n = 4–8 and X = Cl, Br, and I) depending on the length of the organic chain and halogen, we can con-clude that all two-dimensional crystals formed from corner-sharing octahedra. In the one-dimensional crystal $(C_7)DAPbI_4$, there is a detached group of three octahedra connected by common planes. In the one-dimensional crystal $(C_5)DAPbI_4$, there is a detached group of double triples (three octahedra are face-sharing connected) connected with each other by common edges.

Table 4 shows how the halogen and the length of the organic cation affect the displacement of inorganic octahedral layers relative to each other. It can be seen that the oddity of

Table 4 Types of crystal structures formed in hybrid crystals based on lead halides of the $(C_n)DAPbX_4$ (X = Cl, Br, and I) type

Compound	Types of crystal structures		
	X = Cl	X = Br	X = I
$(C_4)DAPbX_4$	DJ (0;0)	DJ (0;0)	RP $(\frac{1}{2};\frac{1}{2})$
$(C_5)DAPbX_4$	RP $(\frac{1}{2};\frac{1}{2})$	RP $(\frac{1}{2};\frac{1}{2})$	—
$(C_6)DAPbX_4$	DJ (0;0)	DJ (0;0)	DJ (0;0)
$(C_7)DAPbX_4$	RP $(\frac{1}{2};\frac{1}{2})$	???	—
$(C_8)DAPbX_4$	DJ (0;0)	DJ (0;0)	DJ (0;0)

Notation for the table: "???" – no structure for analysis and "—" – not applicable.

the alkyl chain in chlorine, bromine, and iodine crystals manifests itself differently. If for iodine crystals it is manifested in the change of dimensionality (as described above), then in chlorine and bromine crystals it is manifested in the formation of DJ structures in the case of even organic cations and RP structures in the case of odd ones. Thus, the oddity of the organic cation together with the type of anion influences the structure of the formed hybrid crystal.

If we refer to Fig. S28,† we can see that the main difference between even diamines and odd diamines is the location of the amine groups relative to the carbon skeleton; while in even diamines both amine groups are located on the same side of the carbon skeleton, in odd diamines they are located on opposite sides of it.

The effect of zigzag changes on the properties of alkanes depending on their oddity has been known for a long time and has been called the "odd–even effect".[32] In recent work,[33] it was shown that the parity of alkanes is directly related to the density of their packing in the crystal during crystallization, and even-numbered alkanes have denser packing than odd-numbered ones.

In our case, at the ends of the carbon skeleton, there are amino groups, which play an important structure-forming role in the formation of such hybrid crystals due to the formation of bonds between the amino group and the inorganic octahedron.[13,14] Thus, in the cases of even diaminoalkanes, the inorganic layers of octahedra are located above each other without displacement, forming Dion–Jacobson structures, while in the case of odd diaminoalkanes, Ruddlesden–Popper structures are formed with displaced layers of inorganic cations relative to each other.

For iodine crystals, the odd–even effect of the organic cation manifests itself in a different way – in the decrease of dimensionality. Apparently, the reason for this is that the iodine octahedron has larger dimensions compared to other halogens. Another peculiarity of iodine structures based on even organic cations is that while sufficiently short organic cations (see $(C_4)DAPbI_4$ in Table 4) form RP structures, longer organic cations (see $(C_6)DAPbI_4$ and $(C_6)DAPbI_4$ in Table 4) form DJ structures. This appears to be due to the fact that longer organic cations have more degrees of freedom than shorter ones.

In other words, we can say that using the example of hybrid crystals based on lead chlorides, bromides, and iodines and a homologous series of diaminoalkanes of the form $NH_3\text{-}(CH_2)_n\text{-}NH_3$, the manifestation of the odd–even effect in hybrid two-dimensional crystals has been demonstrated for the first time.

In the case of an ideal perovskite crystal lattice, the octahedra are symmetric and undeformed, and they are connected to each other at an angle of 180°, and the atoms of the cation B are located exactly in the center of the octahedra. In real crystals, a disordered inorganic sublattice is often observed, variants of which are shown in Fig. S29.† Thus, the octahedra can be connected to each other at an angle other than 180° (Fig. S29a†). To characterize this type of disorder, we can use the angle φ between the inorganic cations of neighboring octahedra through the connecting anion. The more this angle differs from 180°, the greater the degree of disorder the crystal lattice exhibits.

Other types of disorder will characterize the octahedra themselves, not their connection.

In an ideal octahedron, the central atom should be centered, and accordingly, the angles between all anions located at the vertices of the octahedra, measured through the central atom, should be 90°. In real crystals, it is possible for the central atom to be displaced (Fig. S29b†), causing the angles to be different from 90°. This type of disorder of the crystal lattice is usually[32] characterized by the value σ^2_{oct} determined using the formula:

$$\sigma^2_{oct} = 1/12 * \sum_{i=1}^{i=12} (\alpha_i - 90)^2 \qquad (2)$$

where α_i – ith X–Pb–X angle in each octahedron. When there are multiple unique octahedra in a unit cell, the value of σ^2_{oct} is determined for each octahedron and then averaged.

Another type of disorder is related to the deformation of the octahedra themselves (Fig. S29c†). As can be seen, in this case, the X–Pb–X angles will be straight, but the distance between the central atom and the vertices of the octahedra will be different. This type of disorder of the crystal lattice is usually[34] characterized by the value Δd determined using the formula:

$$\Delta d = 1/6 * \sum_{i=1}^{i=6} (d_i - d_{av})^2 / d_i \qquad (3)$$

where d_i is the length of the ith Pb–X bond and d_{av} is the average bond length in the octahedron. When there are multiple unique octahedra in a unit cell, the values of Δd are counted for each octahedron and then averaged.

The analysis of such disorder of real hybrid crystals is very important because they affect, among other things, the optical properties of materials. Thus, it was shown in ref. 35 that the inclination of octahedra relative to each other (the angle φ) affects the width of the bandgap of perovskites, whereas the deformation of the octahedra themselves (σ^2_{oct} and Δd) affects the presence of broadband luminescence in the crystal.[34]

Table 5 summarizes the disorder parameters of the inorganic sublattice of various investigated hybrid compounds based on lead halides of the $(C_n)DAPbX_4$ type. The average bond length of the lead–halogen bond inside octahedra increases in the chlorine–bromine–iodine series; while for chlorine crystals, the average bond length is 2.85–2.88 Å, for bromine crystals, it is from 2.99 to 3.05 Å, and for iodine crystals, it is from 3.2 to 3.24 Å. No correlation is seen between the average bond length in the octahedron and the size or oddity of the organic cation. The displacement of the central atom in the octahedra, σ^2_{oct}, determined from formula (2), shows significant disorder of the corresponding species in the $(C_5)DAPbCl_4$ crystal.

Table 5 Disorder parameters of the inorganic sublattice of hybrid compounds based on lead halides of the (C$_n$)DAPbX$_4$ type

Compound	d_{av}, Å	$\Delta d \times 10^{-3}$, Å^2	σ_{oct}^2, $^{0\,2}$	φ_{av}, ^{0}
(C$_4$)DAPbCl$_4$	2.88	12.42	28.85	150.9
(C$_5$)DAPbCl$_4$	2.86	2.685	231.62	145.83
(C$_6$)DAPbCl$_4$	2.87	10.18	33.19	149.41
(C$_7$)DAPbCl$_4$	2.85	5.45	0.07	145.24
(C$_8$)DAPbCl$_4$	2.87	3.83	15.35	146.62
(C$_4$)DAPbBr$_4$	3.0	5.25	8.01	148.36
(C$_5$)DAPbBr$_4$	2.99	9.53	31.52	150.53
(C$_6$)DAPbBr$_4$	3.05	6.56	40.27	149.29
(C$_7$)DAPbBr$_4$	—	—	—	—
(C$_8$)DAPbBr$_4$	2.99	0.73	3.59	148.21
(C$_4$)DAPbI$_4$	3.2	1.99	3.82	147.18
(C$_5$)DAPbI$_4$	3.23	17.96	22.22	77.85
(C$_6$)DAPbI$_4$	3.21	5.29	2.97	148.47
(C$_7$)DAPbI$_4$	3.24	20.965	34.39	78.16
(C$_8$)DAPbI$_4$	3.2	1.79	7.18	147.62

It has been shown previously that chlorine and bromine hybrid crystals, whose structure contains an organic cation with an odd number of carbon atoms, form inorganic layers displaced relative to each other by $\frac{1}{2}$ the width of the octahedron in the x and y directions. If we exclude them from consideration, the correlation between σ_{oct}^2 and the tilt of the octahedra relative to each other ($180 - \varphi_{av}$) shown in Fig. 16 is illustrative. In this figure, the $180 - \varphi_{av}$ value is used to show the degree of imperfection of the crystal lattice: the more the angle between the octahedra differs from $180°$, the more imperfect crystals are formed.

The application of correlation analysis methods to the data shown in Fig. 16 allows us to determine the Pearson coefficient and, according to it, the presence and strength of correlation between the two types of disordered octahedra. The Pearson coefficient is -0.746, which allows us to state that there is a strong inverse correlation between the two types of disordered
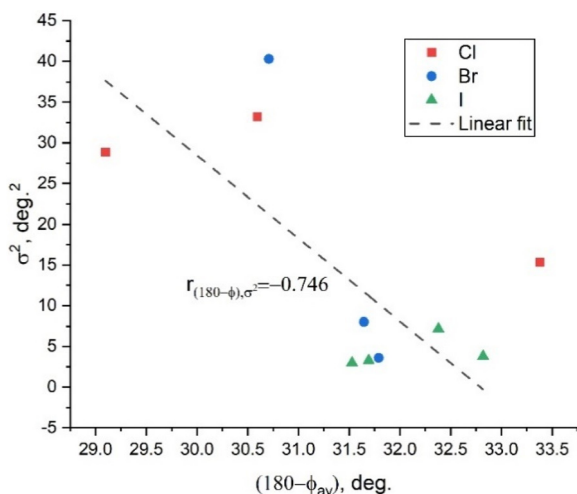
octahedra: internal, characterized by the parameter σ_{oct}^2 and external, characterized by the parameter φ_{av}.

That is, during the formation of the studied hybrid crystals, two competing processes of disorder of the inorganic sublattice are observed, between which a strong negative correlation is found. This confirms the assumptions put forward earlier[14] using the example of studying a narrower sample of similar hybrid crystals.
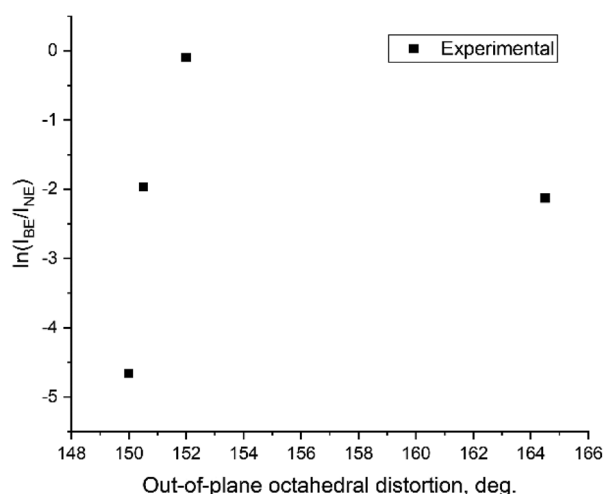
In ref. 12, it was suggested that the ratio between the intensities of narrowband and broadband luminescence is determined by the degree of out-of-plane octahedral distortion. However, this assumption was made based on rather organic cations with heterogeneous structures. In this work, we have an opportunity to test this hypothesis in a homologous series of alkane diamines. Table 6 presents the results of the determination of out-of-plane octahedral distortion for bromine crystals with organic cations of different lengths by the method described in ref. 12.

Fig. 17 shows the relationship between out-of-plane octahedral distortion and the ratio of narrow- and broad-band luminescence in bromine hybrid crystals of the (C$_n$)DAPbBr$_4$ type on a logarithmic scale, as proposed in ref. 12.

It can be seen that there is no correlation between the ratio of narrow- and broad-band luminescence and the degree of disorder of the octahedra of the inorganic sublattice. Thus, it is obvious that there is another mechanism of the influence of the organic cation structure on the luminescence properties of hybrid crystals, different from that proposed in ref. 12.

Table 6 Out-of-plane octahedral distortion in hybrid compounds based on lead halides such as (C$_n$)DAPbBr$_4$

Organic cation length (n):	$n = 4$	$n = 5$	$n = 6$	$n = 7$	$n = 8$
φ_{out},^{0}	150	164.5	150.5	—	152

Fig. 16 Correlation between disorder within octahedra σ_{oct}^2 and the tilt of octahedra relative to each other ($180 - \varphi_{av}$) for hybrid crystals of different cationic and anionic compositions.

Fig. 17 Relationship between out-of-plane octahedral distortion and the ratio of narrow- to broad-band luminescence in bromine hybrid crystals like (C$_n$)DAPbBr$_4$.
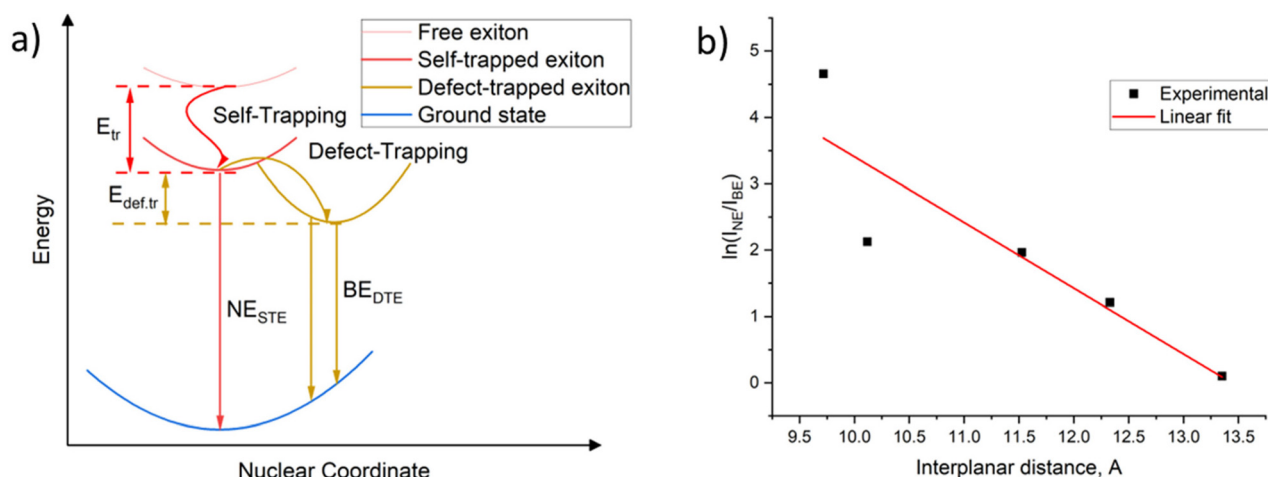
Fig. 18 Energy diagram of the formation of different types of excitons and their corresponding radiative transitions (a), as well as the relationship between the ratio of narrow- to broad-band luminescence and the spacing between layers of inorganic octahedra in bromine hybrid crystals of the (C_n)DAPbBr$_4$ type (b).

It seems to us that it can be as follows (Fig. 18a). Upon photoexcitation of bromine hybrid crystals, free excitons are formed and then autolocalized with the autolocalization energy E_{tr} (arrow "Self-Trapping" in Fig. 18a). Autolocalized excitons can recombine radiatively, which is manifested by narrow-band luminescence (arrow "NE$_{STE}$" in Fig. 18a) and can localize on defects in the crystal lattice of the hybrid crystal with the localization energy $E_{def.tr}$ (arrow "Defect-Trapping" in Fig. 18a). Such excitons localized on defects can also recombine radiatively, which is manifested by broadband luminescence (BE$_{DTE}$ arrows in Fig. 18a).

The number of defects that can be formed in the crystal structure of hybrid 2D materials will increase as the distance between octahedra increases due to the decrease in the interaction between them and the increase in the number of degrees of freedom of the organics separating them. This means that as the distance between inorganic planes increases, the number of excitons recombining through localization at defects should also increase. Fig. 18b shows how the ratio between the intensities of narrowband (STE) and broadband (DTE) luminescence depends on the distance between the layers of inorganic octahedra in bromine hybrid crystals. A clear correlation between these parameters can be seen to be almost linear in nature, which is a strong argument in support of our assumption.

The second important point that requires clarification is the presence of exclusively broadband luminescence in the chlorine crystals under consideration, whereas in bromine (all of the crystals under consideration) and iodine (even) crystals both types of luminescence – narrowband and broadband – are present. Apparently, this is due to the dependence of the energy barrier $E_{def.tr}$ (see Fig. 18a) on the anion: for chlorine crystals this energy barrier is minimal and surmountable already at liquid nitrogen temperature, whereas for bromine and iodine crystals this barrier is larger.

5. Conclusions

The following key results were obtained in the course of this work.

The crystal structure of a new hybrid crystal based on lead chloride, 1,7-heptadiamine and 1,8-octadiamine has been described for the first time.

The manifestation of the odd–even effect in the unit cell structure, band structure and luminescence properties of hybrid crystals with organic cations represented by diaminoalkanes and inorganic sublattices represented by lead halides has been found and analyzed for the first time.

For chlorine and bromine crystals, the odd–even effect in the crystal lattice structure is manifested as follows: even alkanes in the structure of the organic cation contribute to the formation of two-dimensional hybrid crystals with layers of inorganic octahedra located above each other without displacement, while odd alkanes contribute to the formation of two-dimensional hybrid crystals with layers of inorganic octahedra displaced relative to each other by half the width of the octahedron.

For iodine crystals, the odd–even effect in the lattice structure manifests itself differently: even-numbered alkanes in the structure of the organic cation promote the formation of two-dimensional hybrid crystals, whereas odd-numbered alkanes promote the formation of one-dimensional structures.

The odd–even effect in the band structure is manifested as follows: all two-dimensional crystals (all chlorine and bromine, as well as iodine with an even number of carbon atoms in the structure of the organic cation) are direct-band semiconductors with preferential transitions $\Gamma \rightarrow \Gamma$. In turn, iodine crystals with an odd number of carbon atoms in the structure of the organic cation, forming one-dimensional structures, are indirect-band semiconductors.

The odd–even effect on luminescence properties is manifested in the fact that iodine crystals with an odd number of carbon atoms in the organic cation do not have luminescence properties.

It is shown that during the formation of hybrid crystals on the basis of diaminoalkanes, two competing processes of disorder of the inorganic sublattice are observed: internal, characterized by the distortion of the shape of each octahedron or the displacement of lead atoms in octahedra from the central position, and external, characterized by the preservation of the relative perfection of the octahedra themselves, but manifested in the inclination of octahedra relative to each other when they are combined into a network.

The regularities of the influence of the anion as well as the length of the organic cation on the luminescence properties of hybrid crystals are described and investigated in detail for the first time.

For chlorine crystals, only the broadband luminescence of autolocalized excitons is characteristic. Bromine and iodine crystals are characterized by the presence of two types of luminescence: narrow-band luminescence of free excitons and broadband luminescence of autolocalized excitons.

For bromine crystals, the ratio of luminescence intensities of free and autolocalized excitons depends on the size of the organic cation and decreases with its growth.

For iodine crystals, the position of the free exciton luminescence band depends on the length of the organic cation and shifts to the region of shorter wavelengths as it grows.

Author contributions

M.B.: data curation, formal analysis, investigation, visualization, and writing – original draft. A.E.: funding acquisition, resources, validation, and writing – review & editing. D.S.: project administration, conceptualization, funding acquisition, methodology, validation, writing – original draft, and writing – review & editing.

Data availability

Crystallographic data for $(C_7)DAPbCl_4$ have been deposited at the CCDC under depository numbers 2362771 and can be obtained from **https://www.ccdc.cam.ac.uk**.

Crystallographic data for $(C_8)DAPbCl_4$ have been deposited at the CCDC under depository numbers 2362165 and can be obtained from **https://www.ccdc.cam.ac.uk**.

Conflicts of interest

There are no conflicts to declare.

Acknowledgements

References

1 K. Seham, A. Abdel, K.-O. Gudrun, I. Andrei and R. N. Mozhchil, *Appl. Phys. A*, 2017, **123**, 531.

2 L. Mao, Y. Wu, C. C. Stoumpos, M. R. Wasielewski and M. G. Kanatzidis, *J. Am. Chem. Soc.*, 2017, **139**, 5210–5215.

3 S. Wang, Y. Yao, J. Kong, S. Zhao, Z. Sun, Z. Wu, L. Li and J. Luo, *Chem. Commun.*, 2018, **54**, 4053.

4 S. K. Abdel-Aal and A. Ouasri, *J. Solid State Chem.*, 2022, **314**, 123401.

5 H. Fu, Ch. Jiang, Ch. Luo, H. Lin and H. Peng, *Eur. J. Inorg. Chem.*, 2021, **2021**(47), 4984–4989.

6 Z. Kang, H. Xiong, B. Wu, L. Jiang, B. Fan, A. Yang, B. Sa, J. Li, L. Lin and Y. Qiu, *EcoMat*, 2022, **4**(2), e12163.

7 M. Thierry, These, L'universite bordeaux I, 1996, p. 252.

8 G. A. Mousdis, G. C. Papavassiliou, C. P. Raptopoulou and A. Terzis, *J. Mater. Chem.*, 2000, **10**, 515–518.

9 A. Lemmerer and D. G. Billing, *CrystEngComm*, 2012, **14**, 1954–1966.

10 D. G. Billing and A. Lemmerer, *Acta Crystallogr., Sect. C: Cryst. Struct. Commun.*, 2004, **60**, m224–m226.

11 C. Courseille, N. B. Chanh, Th. Maris, A. Daoud, Y. Abid and M. Laguer, *Phys. Status Solidi A*, 1994, **143**, 203–214.

12 M. D. Smith, A. Jaffe, E. R. Dohner, A. M. Lindenberg and H. I. Karunadasa, *Chem. Sci.*, 2017, **8**(6), 4497–4504.

13 M. I. Balanov, O. A. Brylev, V. V. Korochencev, R. Kevorkyants, A. V. Emeline, N. I. Selivanov, Y. V. Chizhov, A. V. Syuy and D. S. Shtarev, *Dalton Trans.*, 2023, **52**, 6388–6397.

14 D. Shtarev, M. Balanov, A. Mayor, A. V. Gerasimenko, R. Kevorkyants, D. Zharovov, K. M. Bulanin, D. Pankin, A. Rudakova, D. Chaplygina, N. I. Selivanov and A. Emeline, *J. Mater. Chem. C*, 2024, **12**, 262–275.

15 Bruker, *APEX 2*, BrukerAXS Inc., Madison, Wisconsin, USA, 2008.

16 G. Kresse and D. Joubert, *Phys. Rev. B: Condens. Matter Mater. Phys.*, 1999, **59**, 1758–1775.

17 J. P. Perdew, K. Burke and M. Ernzerhof, *Phys. Rev. Lett.*, 1996, **77**, 3865–3868.

18 J. P. Perdew, K. Burke and M. Ernzerhof, *Phys. Rev. Lett.*, 1997, **78**, 1396.

19 G. Kresse and J. Hafner, *Phys. Rev. B: Condens. Matter Mater. Phys.*, 1993, **47**, 558–561.

20 G. Kresse and J. Hafner, *Phys. Rev. B: Condens. Matter Mater. Phys.*, 1994, **49**, 14251–14269.

21 G. Kresse and J. Furthmüller, *Comput. Mater. Sci.*, 1996, **6**, 15–50.

22 G. Kresse and J. Furthmüller, *Phys. Rev. B: Condens. Matter Mater. Phys.*, 1996, **54**, 11169–11186.

23 H. J. Monkhorst and J. D. Pack, *Phys. Rev. B: Condens. Matter Mater. Phys.*, 1976, **13**, 5188–5192.

24 T. Williams, C. Kelley, E. A. Merritt, C. Bersch, H.-B. Bröker, J. Campbell, R. Cunningham, D. Denholm, G. Elber, R. Fearick, C. Grammes, L. Hart, L. Hecking, P. Juhász, T. Koenig, D. Kotz, E. Kubaitis, R. Lang, T. Lecomte, A. Lehmann, J. Lodewyck, A. Mai, B. Märkisch, P. Mikulík, D. Sebald, C. Steger, S. Takeno, T. Tkacik, J. van der Woude, J. R. van Zandt, A. Woo and J. Zellner, *Gnuplot 5.2: An interactive plotting program*, 2018.

25 K. Momma and F. J. Izumi, *J. Appl. Crystallogr.*, 2008, **41**, 653–658.

26 https://www.crystallography.net/cod/.

27 J. A. McNulty and P. Lightfoot, *IUCrJ*, 2021, **8**(4), 485–513.

28 A. B. Garg, D. Vie, P. Rodriguez-Hernandez, A. Munoz, A. Segura, D. Errandonea and J. Phys, *Chem. Lett.*, 2023, **14**, 1762–1768.

29 D. S. Shtarev, D. A. Chaplygina, O. V. Patrusheva, C. Chen, A. V. Shtareva, C. C. Stoumpos, R. Kevorkyants and A. V. Emeline, *J. Mater. Chem. C*, 2024, **12**, 5596–5607.

30 T. Ouahrani, R. M. Boufatah, M. Benaissa, A. Morales-García, M. Badawi and D. Errandonea, *Phys. Rev. Mater.*, 2023, **7**, 025403.

31 H. Xue, Z. Chen, S. Tao and G. Brocks, *ACS Energy Lett.*, 2024, **9**(5), 2343–2350.

32 A. Baeyer, *Ber. Dtsch. Chem. Ges.*, 1877, **10**, 1286–1288.

33 K. Yang, Z. Cai, A. Jaiswal, M. Tyagi, J. S. Moore and Y. Zhang, *Angew. Chem., Int. Ed.*, 2016, **55**, 14090–14095.

34 D. Cortecchia, J. Yin, A. Petrozza and C. Soci, *J. Mater. Chem. C*, 2019, **7**, 4956–4969.

35 C. C. Stoumpos and M. G. Kanatzidis, *Acc. Chem. Res.*, 2015, **48**, 2791–2802.